Numerical Investigations of Interhemispheric Asymmetry due to Ionospheric Conductance

R.L. Lysak[1], Y. Song[1], C. L. Waters[2], M. D. Sciffer[3], Y. Obana[4]

[1]School of Physics and Astronomy, University of Minnesota, Minneapolis, USA, [2]School of Mathematical and Physical Sciences, University of Newcastle, NSW, Australia, [3]Pathways and Academic Learning Support Center, University of Newcastle, NSW, Australia, [4]Osaka Electro-Communication University, Neyagawa, Osaka, Japan

Key Points:

- Quarter-wave modes can be excited on magnetic field lines with one footpoint in a sunlit ionosphere and the other footpoint in darkness.
- These wave modes are strongly coupled with cavity resonances in the plasmasphere and magnetosphere
- The quarter-wave modes are found when the ratio of Pedersen conductances between the sunlit and dark ionospheres is greater than 5.

Abstract

Due to differences in solar illumination, a geomagnetic field line may have one footpoint in a dark ionosphere while the other ionosphere is in daylight. This may happen near the terminator under solstice conditions. In this situation, a resonant wave mode may appear which has a node in the electric field in the sunlit (high conductance) ionosphere and an antinode in the dark (low conductance) ionosphere. Thus, the length of the field line is one quarter of the wavelength of the wave, in contrast with half-wave field line resonances in which both ionospheres are nodes in the electric field. These quarter waves have resonant frequencies that are roughly a factor of 2 lower than the half-wave frequency on the field line. We have simulated these resonances using a fully three-dimensional model of ULF waves in a dipolar magnetosphere. The ionospheric conductance is modeled as a function of the solar zenith angle, and so this model can describe the change in the wave resonance frequency as the ground magnetometer station varies in local time. The results show that the quarter-wave resonances can be excited by a shock-like impulse at the dayside magnetosphere and exhibit many of the properties of the observed waves. In particular, the simulations support the notion that a conductance ratio between day and night footpoints of the field line must be greater than about 5 for the quarter waves to exist.

1. Introduction

It is often assumed that the ionospheric signatures of magnetospheric processes are very similar at conjugate points in the northern and southern hemispheres. However, differences between the two hemispheres can occur due to the tilt of the Earth's rotational and magnetic axes, the offset of the magnetic dipole, the orientation of the interplanetary magnetic field (e.g., Østgaard et al., 2011a,b; Tenfjord et al., 2015, 2017), and the asymmetry between the northern and southern ionospheres due to seasonal differences in solar illumination (e.g. Budnik et al., 1998). While all of these effects are important, this study will focus on the seasonal differences in the conjugate ionospheres. In particular, the effects of differing conductivity on wave propagation in the Ultra-Low-Frequency (ULF) range are investigated for solstice conditions when the summer ionosphere is more illuminated than the winter ionosphere.

ULF waves are magnetohydrodynamic (MHD) fluctuations with periods ranging from 0.2-600 seconds (e.g., Kivelson, 1995). In the low beta plasma of the inner magnetosphere ($\beta = 2\mu_0 p/B^2$, where p is the plasma pressure and B is the strength of the geomagnetic field), there are two important ULF wave modes, the shear Alfvén mode that has a group velocity along magnetic field lines and the fast, or compressional, mode whose group velocity may be in any direction (a third mode, the slow mode, is less important in a low-β plasma and disappears completely when $\beta = 0$). The shear Alfvén mode can form standing wave structures known as field line resonances, which extend from one ionosphere to the other (e.g., Cummings et al., 1969; Chen & Hasegawa, 1974; Singer et al., 1981; Takahashi & Anderson, 1992). When both ionospheres are strongly conducting, the electric field of such a wave will be small in the ionosphere, leading to a set of resonances analogous to waves on a string tied down at both ends. The frequency of these waves

depends on the magnetic field line strength, the length of the field line and the amount of mass present along the field line. Therefore, these waves can be used as a diagnostic of the plasma mass density, an area known as magnetoseismology (e.g., Menk & Waters, 2013). On the other hand, the fast mode can exhibit a cavity mode resonance, sometimes called a plasma virtual resonance in the plasmasphere (e.g., Lee & Kim, 1999; Takahashi et al., 2018a,b). A cavity mode can also exist in the outer magnetosphere, particularly on the dayside where the magnetopause produces a sharp boundary to reflect waves (e.g., Kivelson & Southwood, 1986). In the three-dimensional geometry of the magnetosphere, these modes are coupled due to finite gradients in the azimuthal direction (e.g., Zhu & Kivelson, 1988; Allan et al., 1996) and by the ionosphere Hall conductance (e.g., Lysak, 2004; Lysak et al, 2013).

The reflection of ULF waves from the ionosphere depends critically on the ionospheric conductance. When a shear Alfvén wave reflects from the ionosphere, a simple form for the reflection coefficient, defined as the ratio of the electric field of the reflected shear Alfvén wave to the incident wave electric field, is given by (Scholer, 1970; Mallinckrodt & Carlson, 1978) as

$$R_{AA} = \frac{\Sigma_A - \Sigma_P}{\Sigma_A + \Sigma_P} \tag{1}$$

where Σ_P is the effective ionospheric Pedersen conductance and $\Sigma_A = 1/\mu_0 V_A$ is the so-called Alfvén conductance, suitably averaged along the field line. It should be emphasized that this form strictly applies only to the simple case of vertical magnetic field lines, electrostatic electric fields and uniform ionospheric conductance. The Hall conductance and the possible presence of parallel electric fields can be taken into account by suitable modifications of this effective conductance, as outlined by Lysak and Yoshikawa (2006). A more complete description including the Hall conductance as well as finite magnetic zenith angle has been given by Sciffer and Waters (2002) and Sciffer et al. (2004). For field line resonances with a wavelength comparable to the length of the field line, the Alfven conductance can be approximated by using the Alfvén speed at the equator. For example, for an Alfvén speed of 1000 km/s, the Alfvén conductance is 0.8 S, while daytime Pedersen conductance can be much greater than 1 S, so that the reflection coefficient approaches −1 implying that the net ionospheric electric field is nearly zero. On the other hand, at night the Pedersen conductance can be less than 1 S and the wave is more completely absorbed by the ionosphere.

Under some conditions, particularly during the June and December solstices, one footpoint of a geomagnetic field line can be in a sunlit ionosphere while the other footpoint is in darkness. In this case, ULF wave energy is mostly reflected from the sunlit ionosphere and more completely absorbed in the dark ionosphere, producing a tendency for the net Poynting flux of these waves to be directed toward the dark ionosphere. An early study indicating such a trend was performed by Junginger et al. (1985) using data from the geosynchronous GEOS-2 satellite. More recently, attention has focused on so-called quarter-wave modes (e.g., Allan, 1983; Obana et al., 2008, 2015). These modes are formed when the electric field of the wave has a node in the sunlit ionosphere and an anti-node in the dark ionosphere, so that the length of the field line is a quarter of the wavelength of the wave, in contrast with the usual field line resonances with nodes at both ionospheres where the field line length is half the wavelength. Evidence for these modes comes

from the fact that the resonant frequency doubles as the field line moves away from the terminator so that both footpoints are now in sunlight. The quarter-wave modes have lower frequencies and stronger damping than dayside field line resonances, with implications for using the wave frequency for magnetoseismology.

Quarter-wave modes have been modeled in a 2.5-dimensional simulation of the MHD wave equations in a dipole geometry (Obana et al., 2015), with the "half" dimension indicating that the azimuthal dependence of the wave fields can be characterized by a single azimuthal wave number m, with all the wave fields varying as $\exp(im\varphi)$, where φ is the longitude. The purpose of this paper is to extend this previous work to a fully three-dimensional model where a more realistic variation of the ionospheric conductance with local time can be included, and in which the northern and southern ionospheres can be varied to reflect different seasonal conditions. This model is based on the model presented by Lysak et al. (2015), although in this previous model the ionospheric conductances were uniform and the same in both hemispheres.

The remainder of this paper is organized as follows: first, we will describe the model, focusing on the model improvements since the Lysak et al. (2015) paper. Then we will present a study of the response of the magnetosphere to a shock-like impulse from the solar wind under solstice conditions. We will investigate the coupling of cavity modes to both half-wave and quarter-wave field line resonances at different local times and consider the mode structure and ground magnetic fields during daytime and nighttime conditions. The fourth section will consider the response to sinusoidal perturbations, noting in particular differences between a case where the system is driven at the frequency of a plasmasphere cavity mode and a case where it is driven at a non-resonant frequency. The fifth section will examine the effect of varying plasmasphere structure and ionospheric conductivities, and the paper will conclude with a discussion of the important new insights illustrated by these studies.

2. Model description

The model used in this paper is a generalization of the model described in Lysak et al. (2015) and used in Takahashi et al. (2018b) to describe cavity modes in the dayside magnetosphere. The model solves Maxwell's equations using a non-orthogonal dipole grid that conforms to the spherical inner boundary condition at the ionosphere. The region modeled extends from L = 1.5 to L = 10, using a Yee staggered grid with 128 cells in the L-shell dimension, 64 cells in longitude and 318 cells along the field line. The coordinate ν (proportional to 1/L) is directed outward and perpendicular to the background magnetic field, φ is the usual azimuthal coordinate and μ is the field-aligned coordinate, increasing from the southern ionosphere to the north. The spatial resolution along the L = 10 field line varies from 30 km near the ionosphere to 1000 km near the equator. On the other field lines, the coordinate μ is constant so the grid spacing is somewhat smaller. The outer boundary is set to provide reflection on the dayside, modeling the strong Alfvén speed gradient at the magnetopause, while an absorbing boundary condition is used on the nightside, allowing waves to pass through the boundary into the tail region. A fully height-resolved ionosphere is used to model the E-layer and F-layer of the ionosphere, and the inner boundary condition uses an inductive model for the ionosphere (Yoshikawa & Itonaga, 1996; Lysak & Song, 2006) that is more complete than the electrostatic boundary condition used in similar models. This

model solves a Laplace equation for the magnetic scalar potential in the atmosphere that allows for the direct calculation of ground magnetic fields. A full description of this model was presented by Lysak et al. (2015).

The primary extension of this model that is relevant to the present work is the implementation of a structured ionosphere that can consider both sunlit and dark conditions. In previous work (e.g., *Lysak,* 1999), we have considered a variety of ionospheric models that depend on sunlight and magnetic activity, as presented by Kelley (1989). These models are defined by a set of Chapman profiles (Rishbeth & Garriott, 1969) for the ionospheric E, F1, and F2 layers of the form $n = n_0 \exp\left(1 - x - e^{-x}\right)$ where $x = \left(z - z_0\right)/h$. Here z_0 defines location of the peak of the layer and h is a scale height, which can be different above and below the peak. A set of such models was presented by Lysak (1999). Seasonal variations are simulated by placing the subsolar point at different latitudes and basing the ionospheric profile on the solar zenith angle. Two models, one for sunlit conditions and the second for dark conditions are defined, and the transition between them is determined by the hyperbolic tangent, tanh(cos χ/0.1). Figure 1 shows an example of such a profile for equinox conditions where the subsolar point is on the equator. In this figure, the Sun is to the left and dawn is at the top. In this case, the dayside profile is given by model a in Table 1 of Lysak (1999) while the nightside profile is given by model f. It should be emphasized that while Figure 1 shows the height-integrated Pedersen conductivity, the conductivity used in the computations below is distributed with height and also includes the Hall terms.

An example of the model ionospheres under June solstice conditions is presented in Figure 2. This model uses the same dayside parameters but the nightside is given by a profile similar to model f in Table 1 of Lysak (1999) but with the E-layer peak density reduced to 1000 cm^{-3} and the F2 peak reduced to 1.2×10^4 cm^{-3}. The viewpoint in both figures is from the north pole, so that noon is to the left and dawn is at the top in both cases. The notable feature in this figure is that near dawn and dusk, the northern ionosphere is still in daylight while the southern ionosphere is in darkness. This has implications for the formation of field line resonances that will be discussed in the next section.

3. Model results: Shock input

3.1. Equinox conditions

To illustrate the output of the model for a shock-like input and to present a baseline with which to compare later results, we present more detailed results from the run presented in Takahashi et al. (2018b). While that paper focused more on the excitation of plasmaspheric cavity modes by the shock, a set of field line resonances was also excited, as can be seen in Figure 13 of that paper. This figure was taken at 11 MLT, at the location of the Van Allen probes on 15 August 2015. Note that in this run, the plasmapause was placed at L = 5.5 to be consistent with density measurements from the Van Allen Probes. Figure 3a shows the profile of the toroidal electric field at various times during this simulation at 11 MLT and L = 4.5, an L-shell that shows a strong field line resonance (see Figure 13 of Takahashi et al., 2018b). The electric field values are scaled to ionospheric altitudes using the standard dipole mapping that assumes equipotential field lines. However, note that the field lines are not equipotentials in general and this mapping only serves to

compare the electric fields at different altitudes. The field is plotted every 12.5 seconds for this wave, which has a period of about 100 seconds. These fields show the wave form reminiscent of a string tied at both ends due to the high ionospheric conductance at both ends of the field line.

Figure 3b shows a similar plot but taken at 4 MLT. The electric field strength is much less in this nighttime location, and the electric field at the ionosphere is larger relative to the electric field at the equator compared to the wave in Figure 3a due to the lower conductance in the ionosphere at 4 MLT compared to 11 MLT. Higher harmonics can also be seen in this figure, which are weakly present in the dayside case (cf. Figure 13 of Takahashi et al., 2018b), but are overshadowed by the much larger fundamental harmonic. Note also that the presence of only odd harmonics is determined by the symmetric nature of the input source.

Turning to the ground signatures of the waves, Figure 4 shows the Fourier transform of the poleward component of the ground magnetic field variations at a latitude of 62°. It can clearly be seen that the ground signature is much stronger on the dayside than at night, consistent with the observation that FLRs are more commonly seen on the dayside than on the night side (e.g., Waters et al., 1994, 1995). It should be noted that this conclusion depends critically on the assumed ionospheric conductance, as well as on the nature of the driver. For example, in the study of Pi2 pulsations of Lysak et al. (2015), the ionospheric Pedersen conductance (which was assumed to be uniform) was 1.8 S, and field line resonances were clearly seen. This run was also driven with a sinusoidal disturbance with a 50-second period, reminiscent of the oscillatory dipolarization events observed from the THEMIS satellite by Panov et al. (2010, 2013, 2014). This suggests that nightside field line resonances, when they can be observed, are directly driven by an oscillatory perturbation from the tail or occur under circumstances when the nighttime conductivity is relatively high.

3.2 Solstice conditions

We now consider the situation under solstice conditions. We present results from a model run that simulates June solstice conditions, as shown in Figure 2. This run is similar to that presented in Takahashi et al. (2018b), but with the outer (magnetopause) boundary placed at L = 10 and the plasmapause at L = 4. As in the previous run, the system is driven with a shock-like compression in the magnetic field centered on local noon at the equator.

Figure 5 shows the spectrum of the toroidal (E_v) component of the electric field energy density integrated along the field line as a function of invariant latitude and frequency for 11 MLT (Figure 5a) and 06 MLT (Figure 5b). Specifically, the color bar in these figures gives the value of one half the square of the Fourier transform of the electric field divided by the Alfvén speed, integrated along the magnetic field line, which is proportional to the spectral energy density as a function of frequency, with a value of 1 corresponding to 7.96×10^{-4} J/m^2/Hz. The solid line in each of these figures represents the WKB approximation to the field line resonance frequency, while the dashed line gives half of this frequency, which approximates the frequency of the quarter-wave mode. It should be noted that this approximation is not strictly valid for these waves, but it does illustrate the trend in the half-wave resonance frequencies. Furthermore, the structure of the wave fields, as shown in Figures 7, 11, and 12 later in this paper, confirms the nature of the wave modes. The

dayside spectrum follows the field line resonance curve rather well, particularly at lower latitudes where both footpoints are in the high conductivity ionosphere. On the other hand, the spectrum at dawn is not as distinct, owing to the higher damping in the low-conductivity ionosphere. In particular, the strongest waves are at 59° and 68° and about 8 mHz, and lie on the quarter-wave curve.

In the dawn case, it can also be seen that the strongest signals are at 8 mHz and about 22 mHz. Enhancements at these frequencies can also be seen on the dayside. These frequencies correspond to the plasmaspheric cavity mode, as can be seen in Figure 6, which shows the spectrum of the poloidal (E_φ) component at local noon. This component shows the same frequencies at all latitudes, particularly within the plasmasphere (latitudes less than 60°), and the spectrum is unchanged at other local times. This can be compared with Figure 13b of Takahashi et al.(2018b). It should be emphasized that this run was driven with a broad-band source; the enhancements at 8 and 22 mHz are entirely due to the cavity resonance in the system. Comparison with Figure 5 shows that the dayside field line resonances are relatively unaffected by the cavity modes. On the other hand, in the dark ionosphere, only the frequencies associated with the cavity modes are strong enough to be seen clearly in the spectrum.

The quarter wave nature of the mode at 6 MLT can be seen in Figure 7, which shows the electric and magnetic fields at L = 3.7 (invariant latitude 58.7°), corresponding to the 8 mHz resonance seen in Figure 5b. The electric field has an approximate node at the northern (sunlit) end of the field line, while the electric field in the southern (dark) ionosphere shows larger amplitude oscillations. The magnetic field shows the opposite behavior, with larger amplitude magnetic field variations on the dayside than at night. (Note that the sharp drop in the magnetic perturbation near the ionospheres is due to the distributed ionospheric conductivity, which leads to perpendicular currents that decrease the magnetic perturbation.) It is also interesting to see that the northern magnetic field variations maintain the same sign during the oscillation, which can be understood by noting that in the high conductivity ionosphere, the magnetic field of a reflected wave has the same sign as that of the incident wave. The magnetic field in the dark ionosphere is not a perfect node in this case. The Pedersen conductance at this point is 0.24 S, while the equatorial Alfvén speed is about 1000 km/s, giving an Alfvén conductance of 0.80 S. The reflection coefficient for Alfvén waves for a constant Alfvén speed as given by equation (1) is then 0.54, where a value approaching 1.0 would give a node in the magnetic field.

The ground signature of the quarter wave also shows interesting properties. Obana et al. (2015) have shown an increase in the resonance frequency as the magnetometer stations passed from nighttime through dawn. Similar behavior can be seen in Figure 8a, which shows the northward components of the magnetic field observed on the ground at a latitude of 52.8° south, as in the Middlemarch, NZ, station used in Obana et al. (2015). The bottom solid curve is from 06 MLT with the dotted and dashed curves at 09 and 11 MLT, respectively. The zero point of these curves has been offset by 5 nT for clarity. The locations on the dayside show a higher frequency wave, although still modulated at the lower frequency. Figure 8b shows the Fourier transform of the wave fields with the same line styles as in Figure 8a, indicating that the quarter-wave peak at about 8 mHz is much stronger than the 22 mHz wave at 6 MLT, while the half-wave field line resonance

peak at 22 mHz is of comparable amplitude to the 8 mHz peak for the dayside locations. Figure 9 shows the ground magnetic fields on the illuminated end of this field line. It can be seen that while the quarter-wave peak is still dominant at 6 MLT, the higher frequency wave is still relatively strong at 6 MLT in the sunlit hemisphere, indicating that the damping due to the dark ionosphere is significant for this higher frequency wave. This is consistent with the observations of Obana et al. (2015) showing a transition from a lower frequency wave to a higher frequency wave as the southern hemisphere stations pass into daylight.

4. Constant frequency drivers

As we have seen above, the broadband source produces cavity mode oscillations at 8 mHz and 22 mHz. However, in some cases we might expect a nearly monochromatic source at a given frequency. In order to examine the evolution of the system in such a case, runs were performed with drivers at frequencies of 8 mHz and 22 mHz corresponding to the cavity resonances as well as at an off-resonant frequency at 15 mHz. In each case, the driving pulse was modulated with an exponential decay with a time constant of 200 seconds. Figure 10 shows the power spectrum of the electric field energy density at 6 and 11 MLT in each of these cases. In this figure, the left-hand column (panels a, c, and e) give the spectra for 6 MLT while the right-hand column (panels b, d, and f) show the results for 11 MLT. The top row is for the 8 mHz driver, the middle row is 15 mHz and the bottom row is 22 mHz. Note that as in Figure 5, the solid line in each figure represents the WKB approximation to the half-wave mode field line resonance frequency, while the dashed line, at half that frequency, gives the approximate frequency of the quarter-wave mode.

As expected, the dominant response in all cases is at the driving frequency. For the dayside (11 MLT) cases, the spectra show enhancements when the field line resonance frequency matches that of the driver. On the other hand, the fields at dawn (6 MLT) show enhancements at the quarter wave frequency. Analysis of the wave forms, as in Figure 11, confirms the half-wave signature on the dayside and the quarter wave signature at dawn. The 8 mHz and 22 mHz runs show larger amplitudes at those frequencies, while the 15 mHz run not only shows wave power at the driving frequency but also at the 8 mHz and 22 mHz resonances. This is due to the fact that the driving wave form is a damped exponential, and the 200 second decay time implies a 5 mHz bandwidth. Thus, in this run, there is still significant power at the resonant frequencies. It can also be seen that the maximum power is larger for the runs driven at the resonance. (Note that the number given in the title of each panel of Figure 10 is the electric field energy density integrated along the field line in the units defined above in the discussion of Figure 5.)

5. Variations in parameters

5.1 Conductivity variations

The run presented in the previous section was a rather strong conductivity ratio in order to highlight the quarter wave modes (the integrated Pedersen conductance was 13.6 S in the northern hemisphere and 0.266 S in the south at the latitude of Middlemarch, NZ). It is worth considering how large the ratio must be for quarter waves to be seen. This is particularly relevant since Obana et al. (2015) suggested that the quarter wave modes occurred when the ratio of the conductances at conjugate points was greater than 5. To test this hypothesis, results from a series of runs were

examined in which the conductance ratios were 11.1 (13.6 S in summer, 1.22 S in winter), 5.39 (6.57 S in summer, 1.22 S in winter) and 2.07 (13.6 S in summer, 6.57 S in winter). The results are shown in Figure 11, which plots the electric and magnetic field profiles just inside the plasmapause for these three cases, with panels (a) and (b) being the 11.1 ratio case, (c) and (d) are for 5.38 and (e) and (f) are for a ratio of 2.07.

The two runs with higher conductance ratio show characteristics of the quarter-wave solution. This is indicated by the asymmetric pattern of the electric field, with a near node at the summer (northern) ionosphere. The magnetic field is roughly antisymmetric; however, there is not a node at or near the equator, in contrast with the lower conductance ratio case (panel f) where the magnetic field has a node at the equator. The electric field also shows symmetry (panel e), indicative of a half-wave field line resonance.

The runs of Figure 11 all had a very high dayside conductance, leading to a node in the electric field. To test whether the quarter waves still persist in a lower conductance case, Figure 12 shows field profiles as in Figure 11, but with both the dayside and nightside conductivities reduced by roughly a factor of 5. Panels (a) and (b) show the electric and magnetic fields, respectively, for a run with Pedersen conductance of 2.71 S in the north and 0.28 S is the south (ratio of 9.7). Neither ionosphere produces a node in the electric field, which remains positive through the wave cycle. However, the magnetic field variations show an asymmetry, indicated by the lack of an equatorial node in the magnetic field. Panels (c) and (d) (1.27 S in the north and 0.28 in the south, ratio of 4.5) shows a similar pattern, while panels (e) and (f) (2.71 S in the north and 1.38 in the south, ratio of 2.0) shows more symmetric structure with a node in the magnetic field at the equator. Thus, while the resonances are less distinct in these low conductance cases, the general pattern of asymmetry for larger conductance ratios holds.

5.2 Plasmasphere density variations

An important result from the preceding section is that the presence of quarter-wave modes seems directly associated with the presence of cavity mode resonances in the plasmasphere. This dependence suggests considering the effect of variations in the plasmaspheric density. To do this, we have performed runs identical to the one shown in Figures 5 and 6 but with either the density in the plasmasphere increased by a factor of 4 or the density in the magnetospheric cavity outside the plasmapause increased by a factor of 4. These variations reduce the Alfvén speed in the respective regions by a factor of 2, which should also lower the cavity mode frequencies by this factor. Figure 13 shows the spectrum of the poloidal mode electric field for these two cases for runs in which a broad-band input, as in the run shown in Figures 5 to 9. Figure 13a shows the case where the plasmaspheric density was increased. Comparison of this figure with Figure 6 shows that the frequency of the fundamental cavity mode is essentially unchanged, at about 8 mHz. However, the harmonic structure, especially in the plasmasphere, is modified, in particular showing an enhancement at about 13 mHz. It is also interesting to note that the amplitude of the mode inside the plasmasphere is somewhat larger than in Figure 6 (note that the two figures have the same color bar, which is expressed as the base 10 logarithm of the spectral energy density).

Figure 13b shows the case where the outer magnetospheric density is increased. In this case, the cavity modes are less distinct but there is a clear reduction in the fundamental frequency to about 4 mHz, or one half of the frequency in Figure 6. This confirms that the cavity response at low frequencies is primarily associated with the outer magnetospheric region. These results are consistent with previous work (Lee & Lysak, 1994; Waters et al., 2000) showing that the fast mode wave cutoff occurs at larger L for smaller frequencies. Hence, at low frequencies, a cavity mode is evanescent at lower L and is therefore most sensitive to the Alfven speed at larger L. Recall that the outer boundary of the simulation on the dayside has a reflecting boundary, corresponding to the magnetopause, consistent with the sharp decrease in the Alfvén speed in the magnetosheath (outside the simulation domain) since the magnetic field is reduced and the density is increased in this region. These modes are very weak on the nightside, where the outer boundary allows ULF wave energy to pass out of the system down the tail. This also suggests that the enhanced plasmaspheric wave energy shown in Figure 13a relative to Figure 6 may result from a more efficient coupling between the plasmasphere and outer magnetosphere.

6. Discussion and Conclusions

The runs presented here clearly show that quarter-wave modes can be supported in the magnetosphere when one footpoint of a magnetic field line is in darkness while the other is in sunlight. The high-conductance (sunlit) ionosphere stays as an approximate node of the wave electric field while the low-conductance (dark) ionosphere acts more like an anti-node of the electric field. Our results are consistent with the observations of Obana et al. (2015) that showed that the field line resonance frequency increased by approximately a factor of two as the magnetometers moved from darkness to daylight. In addition, our results support the suggestion of Obana et al. (2015) that the ratio of the Pedersen conductances between the sunlit and dark ionospheres should be greater than 5 for the quarter-wave modes to be seen. However, the conductance ratio is only one parameter that may influence the existence of quarter wave modes. Future work will attempt to establish the ionospheric conditions that lead to quarter-wave modes more precisely.

However, the global nature of our simulation allows us to understand the dynamics behind these modes more completely. In particular, cavity mode resonances in the plasmasphere and the dayside magnetosphere play a strong role in the formation of the quarter-wave resonances. Because one footpoint is in darkness, the quarter-wave mode is more strongly damped in this ionosphere. This suggests that the quarter-wave modes are most readily observable when the quarter-wave frequency corresponds to the cavity mode frequency. This differs from the half-wave modes, especially those seen on the dayside, which suffer only weak damping and are not as strongly affected by the cavity mode. One possible exception to this is when the wave is directly driven by an oscillatory source, such as might be expected for periodic solar wind pressure variations (e.g., Sibeck et al., 1989), Kelvin-Helmholtz instabilities (e.g., Engebretson et al., 1998), or periodic bursty bulk flows from the magnetotail (e.g., Panov et al., 2013). However, our results show that even with a periodic driver, the quarter-wave modes are stronger in amplitude when the driving frequency matches a cavity mode resonance.

One aspect of these simulations that does not agree with the observations is the ratio between the frequencies of the half-wave field line resonance and the quarter-wave modes, which was found to be 1.3 to 1.8 by Obana et al. (2015) at the Middlemarch station and is about 2.7 in the simulation. It is somewhat of a coincidence that the quarter-wave frequency also corresponds to the cavity mode frequency in the model, as can be seen by a comparison of Figure 5a and Figure 6. Given the strong influence of the quarter-wave observations on the plasmaspheric cavity resonance, this result may be due to a different density profile in the plasmasphere, modifying the cavity resonance frequency. It is also important to note that the resonance frequency depends on the density in the outer magnetosphere as well as in the plasmasphere, suggesting that the relevant cavity is the whole dayside magnetosphere, with a reflecting boundary at the magnetopause. From the point of view of magnetoseismology, this may indicate that the observation of quarter waves gives information about the density profile in the plasmasphere and outer magnetosphere.

This work has emphasized the difference in ionospheric conductivity in producing interhemispheric differences in ground observations. We have therefore simplified the model to isolate the ionospheric effects. This leaves open a number of questions, such as the role of the azimuthal asymmetry in the plasmaspheric density profile in the observations of these waves. It is well known that there are strong dawn-dusk asymmetries in the plasmapause location, with the plasmapause extending to larger radial distances on the dusk side (e.g., Carpenter, 1966). In addition, plasmaspheric plumes can produce enhanced density on the dusk side extending toward the magnetopause (e.g., Goldstein, 2006). These structures will complicate the signatures of the cavity mode and the field-line resonances that are coupled to them. Investigation of such effects will be the focus of further work.

In summary, this work has established that quarter-wave modes can be excited both by monochromatic drivers and broadband drivers. In the latter case, the quarter waves are strongly excited when they couple effectively to cavity modes in the plasmasphere and magnetosphere. These modes can exist when the conductance ratio between the conjugate footpoints of a field line is 5 or greater. Such conditions can exist near the terminator under solstice conditions. Understanding the conditions under which quarter waves can be excited is critical for using the techniques of magnetoseismology to use field-line resonances to diagnose the density along the field line.

Acknowledgements. Work at the University of Minnesota is supported by grant AGS-1840891 from the National Science Foundation. We also acknowledge supercomputer support from the Minnesota Supercomputer Institute. R.L.L. would like to thank the University of Newcastle, where some of this work was carried out, for its support. Source code for the numerical simulations and data files associated with the results presented in this paper are available at the Data Repository for the University of Minnesota (DRUM) at https://doi.org/10.13020/d1g7-c676.

References

Allan, W. (1983), Quarter-wave ULF pulsations, *Planet. Space Sci., 31*(3), 323–330, doi:10.1016/0032-0633(83)90083-1.

Allan, W., Menk, F. W., Fraser, B. J., Li, Y., & S. P. White (1996), Are low-latitude Pi 2 pulsations cavity/waveguide modes?, *Geophys. Res. Lett., 23*(7), 765.

Budnik, F., Stellmacher, M., Glassmeier, K.-H., & Buchert, S. C. (1998), Ionospheric conductance distribution and MHD wave structure: observation and model, *Ann. Geophys., 16,* 140.

Carpenter, D. L. (1966), Whistler studies of the plasmapause in the magnetosphere, 1, Variations in the position of the knee and some evidence on plasma motions near the knee, *J. Geophys. Res., 71,* 693.

Chen, L., & Hasegawa, A. (1974), A theory of long-period magnetic pulsations, 1, Steady state excitation of field line resonances, *J. Geophys. Res., 79,* 1024.

Cummings, W. D., O'Sullivan, R. J., & Coleman, P. J. (1969), Standing Alfvén waves in the magnetosphere, *J. Geophys. Res., 74,* 778.

Engebretson, M. J., Glassmeier, K.-H., Stellmacher, M., Hughes, W. J., & Lühr, H. (1998), The dependence of high-latitude Pc5 wave power on solar wind velocity and on the phase of high-speed solar wind streams, *J. Geophys. Res., 103,* 26,271, doi: 10.1029/97JA03143.

Goldstein, J. (2006), Plasmasphere response: Tutorial and review of recent imaging results, *Space Sci. Revs., 124,* 203.

Junginger, H., Haerendel, G., & Melzner, F. (1985), A statistical study of wave Poynting vectors measured during long-period magnetospheric pulsations at geostationary orbit, *J. Geophys. Res., 90,* 8301.

Kelley, M. C. (1989), *The Earth's Ionosphere*, Academic Press, Inc.

Kivelson, M. G. (1995), Pulsations and magnetohydrodynamic waves, in *Introduction to Space Physics,* M. G. Kivelson and C. T. Russell (eds.), Cambridge University Press, Cambridge, UK, p. 330.

Kivelson, M. G., & Southwood, D. J. (1986), Coupling of global magnetospheric MHD eigenmodes to field line resonances, *J. Geophys. Res., 91,* 4345.

Lee, D.-H., & Kim, K. (1999), Compressional MHD waves in the magnetosphere: A new approach, *J. Geophys. Res., 104,* 12,379.

Lee, D.-H., & Lysak, R. L. (1994), Numerical studies on ULF wave structures in the dipole model, in *Solar Wind Sources of Magnetospheric Ultra-Low-Frequency Waves,* M. Engebretson, K. Takahashi and M. Scholer (eds.), Geophysical Monograph 81, American Geophysical Union, Washington, p. 293.

Lysak, R. L. (1999), Propagation of Alfvén waves through the ionosphere: Dependence on ionospheric parameters, *J. Geophys. Res., 104,* 10,017.

Lysak, R. L. (2004), Magnetosphere-ionosphere coupling by Alfvén waves at midlatitudes, *J. Geophys. Res.*, 109, A07201, doi:10.1029/2004JA010454.

Lysak, R. L., & Song, Y. (2006), Magnetosphere-ionosphere coupling by Alfvén waves: Beyond current continuity, *Adv. Space Res.,38*(8)*,* 1713.

Lysak, R. L., Song, Y., Sciffer, M. D., & Waters, C. L. (2015), Propagation of Pi2 pulsations in a dipole model of the magnetosphere*, J. Geophys. Res. Space Physics, 120,* doi:10.1002/2014JA020625.

Lysak, R. L., Waters, C. L., & Sciffer, M. D. (2013), Modeling of the ionospheric Alfvén resonator in dipolar geometry, *J. Geophys. Res. Space Physics, 118,* doi: 10.1002/jgra.50090.

Lysak, R. L., & Yoshikawa, A. (2006), Resonant cavities and waveguides in the ionosphere and atmosphere, in *Magnetospheric ULF Waves: Synthesis and New Directions,* K. Takahashi, P. J. Chi, R. E. Denton, and R. L. Lysak (eds.), AGU Geophysical Monograph 169, American Geophysical Union, Washington, p. 289.

Mallinckrodt, A. J., & Carlson, C. W. (1978), Relations between transverse electric fields and field-aligned currents, *J. Geophys. Res., 83,* 1426.
Menk, F. W., & Waters, C. L. (2013), *Magnetoseismology*, Wiley-VCH, Weinheim, Germany.
Obana, Y., Menk, F. W., Sciffer, M. D., & Waters, C. L. (2008), Quarter-wave modes of standing Alfvén waves detected by cross-phase analysis, *J. Geophys. Res., 113,* A08203, doi:10.1029/2007JA012917.
Obana, Y., Waters, C. L., Sciffer, M. D., Menk, F. W., Lysak, R. L., Shiokawa, K., et al. (2015), Resonance structure and mode transition of quarter-wave ULF pulsations around the dawn terminator, *J. Geophys. Res. Space Physics, 120,* 4194–4212, doi:10.1002/2015JA021096.
Østgaard, N., Humberset, B. K., & Laundal, K. M. (2011a), Evolution of auroral asymmetries in the conjugate hemispheres during two substorms, *Geophys. Res. Lett., 38,* L03101, doi:10.1029/2010GL046057.
Østgaard, N., Laundal, K. M., Juusola, L., Åsnes, A., Håland, S. E., & Weygand, J. M. (2011b), Interhemispherical asymmetry of substorm onset locations and the interplanetary magnetic field, *Geophys. Res. Lett., 38,* L08104, doi:10.1029/2011GL046767.
Panov, E. V., Baumjohann, W., Nakamura, R., Amm, O., Kubyshkina, M. V., Glassmeier, K.-H., et al. (2013), Ionospheric response to oscillatory flow braking in the magnetotail, *J. Geophys. Res. Space Physics, 118,* 1529–1544, doi:10.1002/jgra.50190.
Panov, E. V., Baumjohann, W., Nakamura, R., Kubyshkina, M. V., Glassmeier, K.-H., Angelopoulos, V., et al. (2014), Period and damping factor of Pi2 pulsations during oscillatory flow braking in the magnetotail, *J. Geophys. Res. Space Physics, 119,* doi:10.1002/2013JA019633.
Panov, E. V., Nahamura, R., Baumjohann, W., Angelopoulos, V., Petrukovich, A. A., Retino, A., et al. (2010), Multiple overshoot and rebound of a bursty bulk flow, *Geophys. Res. Lett., 37,* L08103, doi:10.1029/2009GL041971.
Rishbeth, H., & Garriott, O. K. (1969), *Introduction to Ionospheric Physics,* Academic Press, New York.
Scholer, M. (1970), On the motion of artificial ion clouds in the magnetosphere, *Planet. Space Sci., 18,* 977.
Sciffer, M. D., & Waters, C. L. (2002), Propagation of ULF waves through the ionosphere: Analytic solutions for oblique magnetic fields, *J. Geophys. Res., 107*(A10), 1297, doi: 10.1029/2001JA000184.
Sciffer, M. D., Waters, C. L., & Menk, F. W.(2004), Propagation of ULF waves through the ionosphere: Inductive effect for oblique magnetic fields, *Ann. Geophys., 22,* 1155.
Sibeck, D. G., Baumjohann,, W. Elphic, R. C., Fairfield, D. H., Fennell, J. F., Gail, W. B., et al. (1989), The magnetospheric response to 8-minute period strong-amplitude upstream pressure variations, *J. Geophys. Res., 94,* 2505.
Singer, H. J.., Southwood, D. J., Walker, R. J., & Kivelson, M. G. (1981), Alfvén wave resonances in a realistic magnetospheric magnetic field geometry, *J. Geophys. Res., 86,* 4589.
Takahashi, K., & Anderson, B. J. (1992), Distribution of ULF energy ($f < 80$ mHz) in the inner magnetosphere: A statistical analysis of AMPTE CCE magnetic field data, *J. Geophys. Res., 97,* 10,751.
Takahashi, K., Hartinger, M. D., Vellante, M., Heilig, B., Lysak, R. L., Lee, D.-H., & Smith, C. W. (2018a), Roles of flow braking, plasmaspheric virtual resonances, and ionospheric

currents in producing ground Pi2 pulstaions, *J. Geophys. Res. Space Physics, 123*, 9187–9203, doi: 10.1029/2018JA025664

Takahashi, K., Lysak, R. L., Vellante, M., Kletzing, C. A., Hartinger, M. D., & Smith, C. W. (2018b), Observation and numerical simulation of cavity mode oscillations excited by an interplanetary shock, *J. Geophys. Res. Space Physics, 123*, 1969, doi: 10.1002/2017JA024639.

Tenfjord, P., Østgaard, N., Snekvik, K., Laundal, K. M., Reistad, J. P., Haaland, S., & Milan, S. E. (2015), How the IMF By induces a By component in the closed magnetosphere and how it leads to asymmetric currents and convection patterns in the two hemispheres, *J. Geophys. Res. Space Physics, 120,* 9368–9384, doi:10.1002/2015JA021579.

Tenfjord, P., Østgaard, N., Strangeway, R., Haaland, S., Snekvik, K., Laundal, K. M., et al. (2017), Magnetospheric response and reconfiguration times following IMF By reversals, *J. Geophys. Res. Space Physics, 122,* 417–431, doi:10.1002/2016JA023018.

Yoshikawa, A., & Itonaga, M. (1996), Reflection of shear Alfvén waves at the inductive ionosphere, *Geophys. Res. Lett., 23,* 101.

Waters, C. L., Harrold, B. G., Menk, F. W., Samson, J. C., Fraser, B. J. (2000), Field line resonance and waveguide modes at low latitudes 2. A model, *J. Geophys/ Res., 105,* A4, 7763-7774.

Waters, C. L., Menk, F. W., & Fraser, B. J. (1994), Low latitude geomagnetic field line resonance: Experiment and modeling, *J. Geophys. Res., 99,* 17,547.

Waters. C. L., Samson, J. W., & Donovan, E. F. (1995), The temporal variation of the frequency of high latitude field line resonances, *J. Geophys. Res., 100,* 7987.

Zhu, X. M., & Kivelson, M. G. (1988), Analytic formulation and quantitative solutions of the coupled ULF wave problem, *J. Geophys. Res., 93,* 8602.

Figure Captions

Figure 1. Contours of height-integrated Pedersen conductance for equinox conditions.

Figure 2. Height-integrated Pedersen conductance for June solstice conditions. (a) Northern hemisphere; (b) Southern hemisphere

Figure 3. Profiles of the electric field taken at intervals of 12.5 seconds at L = 4.5 and MLT of (a) 11; (b) 4. Field line resonance structure is clear in daytime case, weaker and less clearly structured at night. All fields are scaled to ionospheric values.

Figure 4. Fourier transform of the ground magnetic field at a latitude of 62° as a function of magnetic local time. Note that the strongest ground fields are during the daytime hours, MLT = 6 to 18.

Figure 5. Energy density in the toroidal electric field component, integrated along the magnetic field line, as a function of frequency and invariant latitude. Solid line gives the WKB estimate for the field line resonance frequency, while the dashed line gives an estimate of the quarter-wave frequency (a) 11 MLT, field line resonances are dominant; (b) 6 MLT, signatures are weaker and strongest at the cavity mode frequencies.

Figure 6. Energy density in the poloidal component of the electric field, showing the cavity mode nature of these oscillations. Note that the cavity mode is not strictly confined to the plasmasphere and in fact leaks out to the outer magnetosphere.

Figure 7. Wave forms of the (a) electric and (b) magnetic fields of the toroidal oscillation as a function of latitude along the magnetic field lines. Note that the fields have been scaled to their ionospheric values.

Figure 8. (a) Ground magnetic fields at 52.8° latitude in the southern (dark) ionosphere. The solid line is at 6 MLT, the dotted line at 9 MLT and the dashed line at 11; (b) Fourier transforms of these fields.

Figure 9. Same as Figure 8, but for the fields in the northern (sunlit) hemisphere.

Figure 10. Energy density in the toroidal electric field at 6 MLT (panels a,c, and e) and 11 MLT (panels b, d, and f). Panels (a) and (b) are for a driving frequency of 8 mHz; panels (c) and (d) for 15 mHz and panels (e) and (f) for 22 mHz.

Figure 11. Effect of varying the conductance ratio. Panels (a) and are for a ratio of 11.1, (c) and (d) for 5.4 and (e) and (f) for 2.1. Left column gives the electric field and right column the magnetic field.

Figure 12. Similar to Figure 11 but for lower conductance values.

Figure 13. Poloidal energy density in the electric field integrated along the field line for runs in which (a) the plasmaspheric density is increased by a factor of 4, and (b) the outer magnetospheric density is increased by a factor of 4. Note that both modifications affect the energy spectrum; however the frequency decrease is more pronounced in the second case.

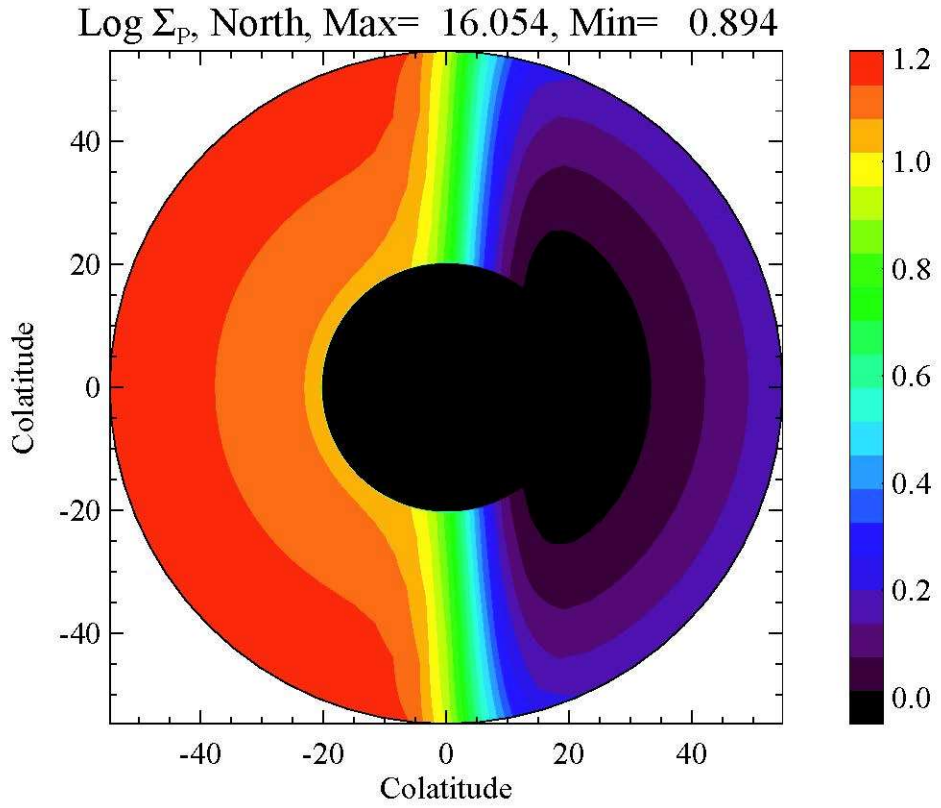

Figure 1. Contours of height-integrated Pedersen conductance for equinox conditions.

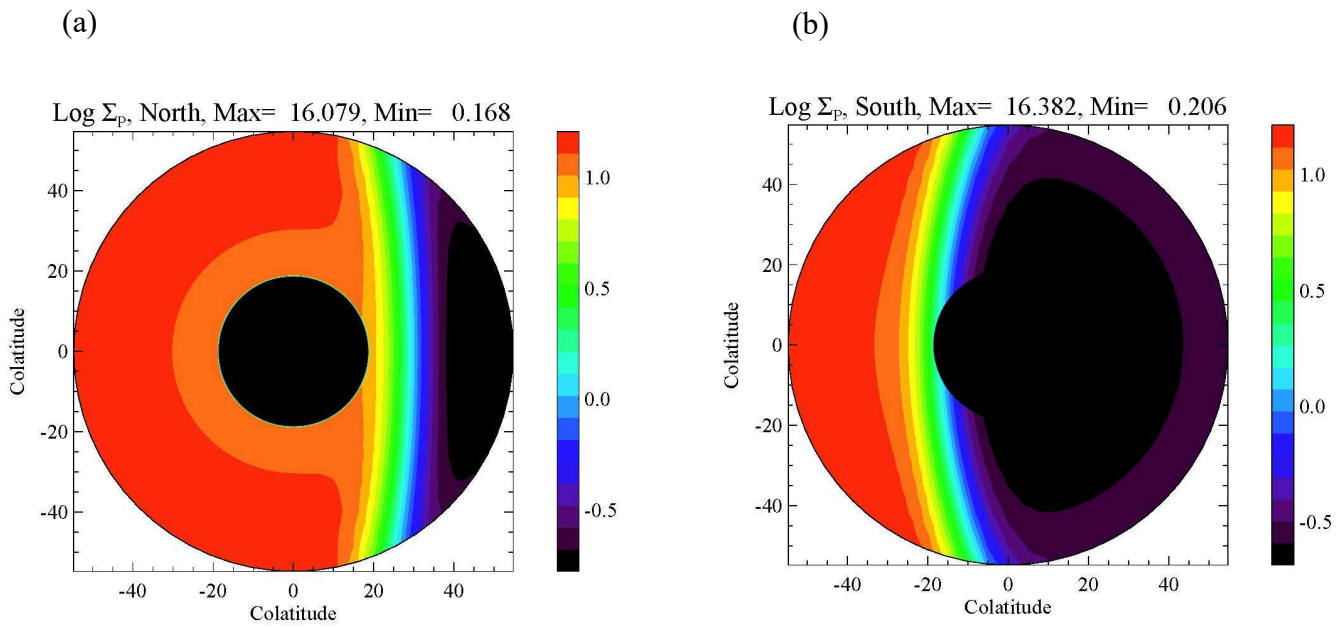

Figure 2. Height-integrated Pedersen conductance for June solstice conditions. (a) Northern hemisphere; (b) Southern hemisphere

(a)

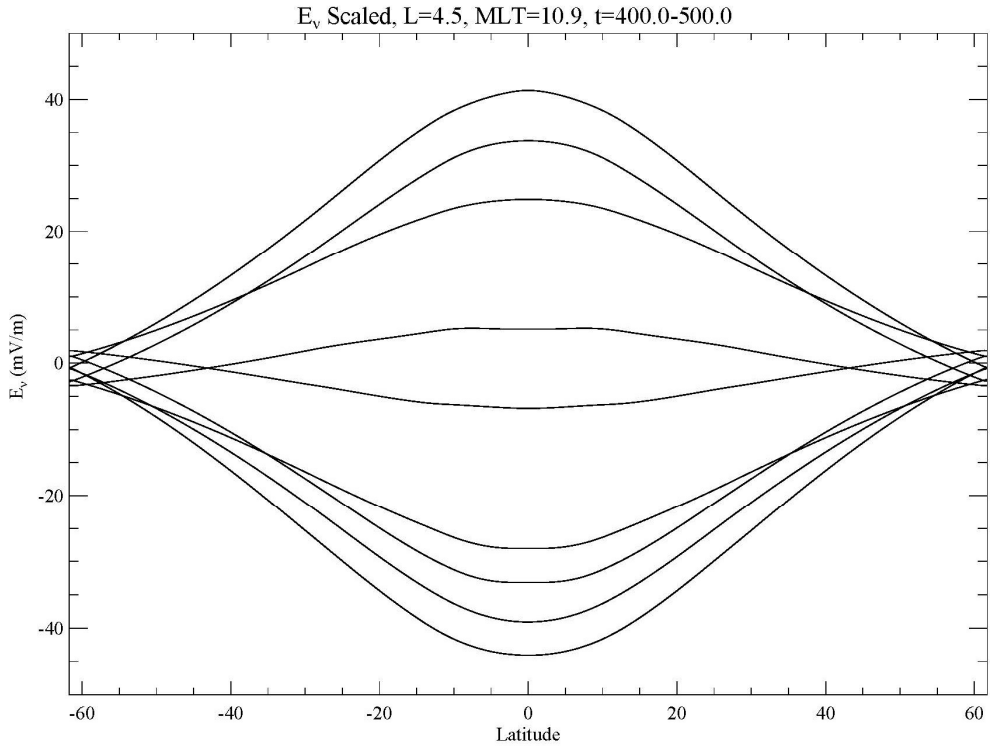

(b)

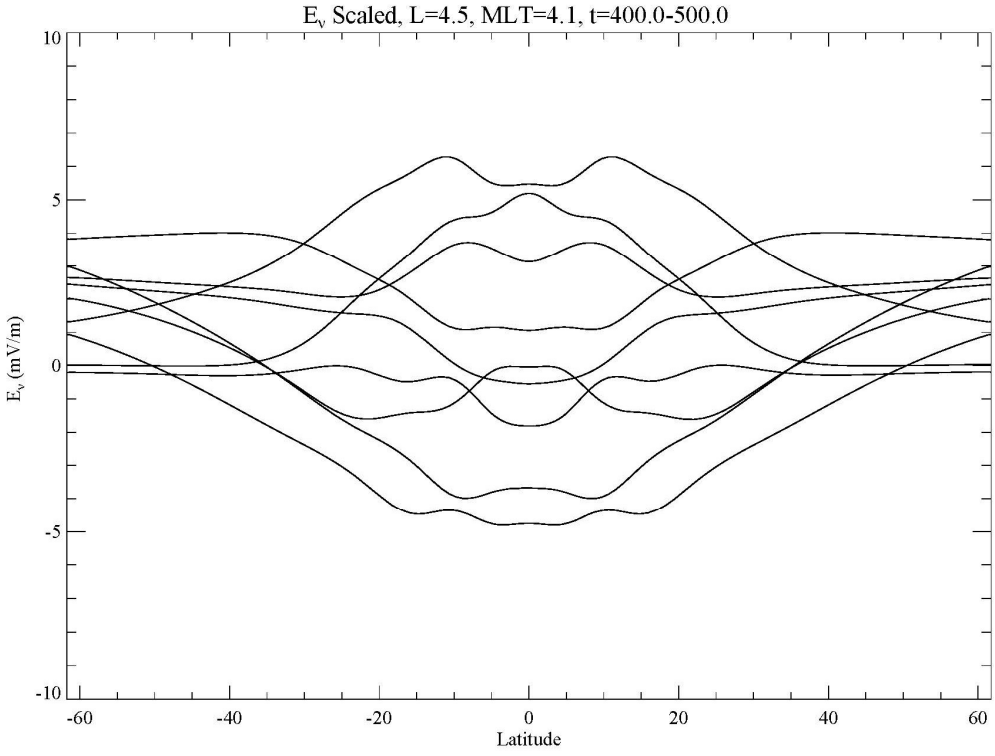

Figure 3. Profiles of the electric field taken at intervals of 12.5 seconds at L = 4.5 and MLT of (a) 11; (b) 4. Field line resonance structure is clear in daytime case, weaker and less clearly structured at night. All fields are scaled to ionospheric values.

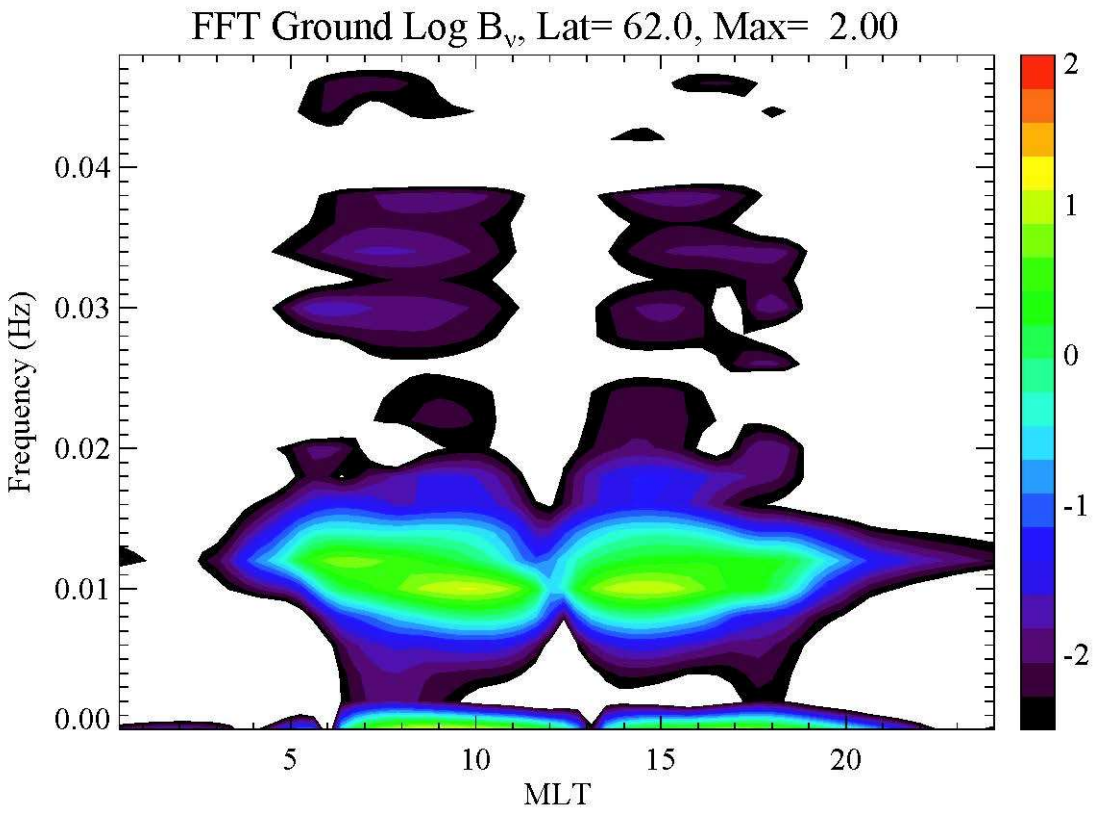

Figure 4. Fourier transform of the ground magnetic field at a latitude of 62° as a function of magnetic local time. Note that the strongest ground fields are during the daytime hours, MLT = 6 to 18.

(a)

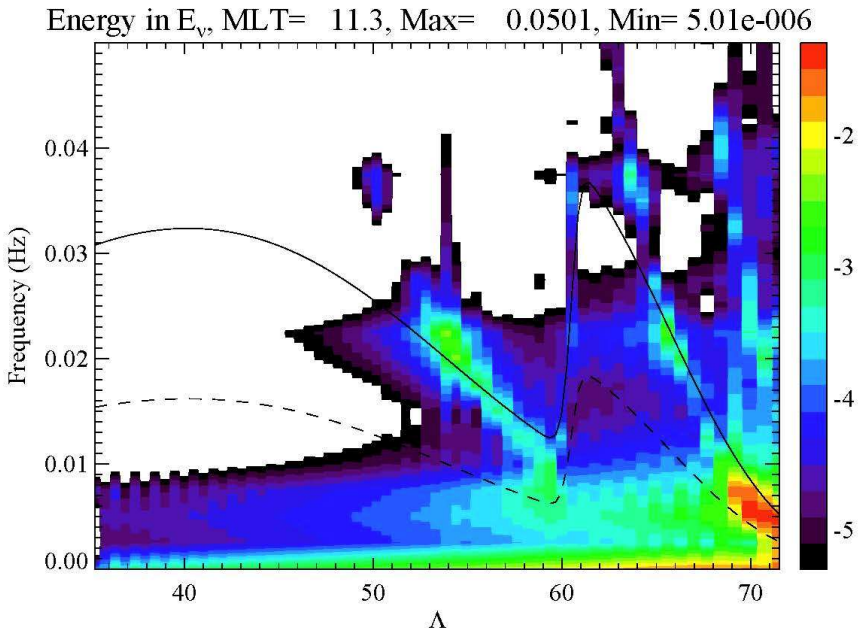

(b)

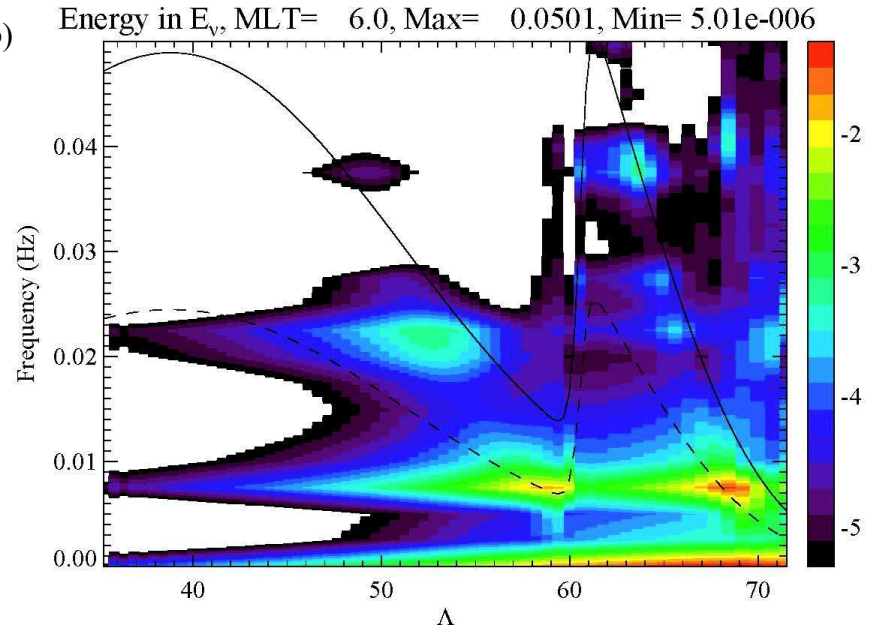

Figure 5. Energy density in the toroidal electric field component, integrated along the magnetic field line, as a function of frequency and invariant latitude. Solid line gives the WKB estimate for the field line resonance frequency, while the dashed line gives an estimate of the quarter-wave frequency (a) 11 MLT, field line resonances are dominant; (b) 6 MLT, signatures are weaker and strongest at the cavity mode frequencies.

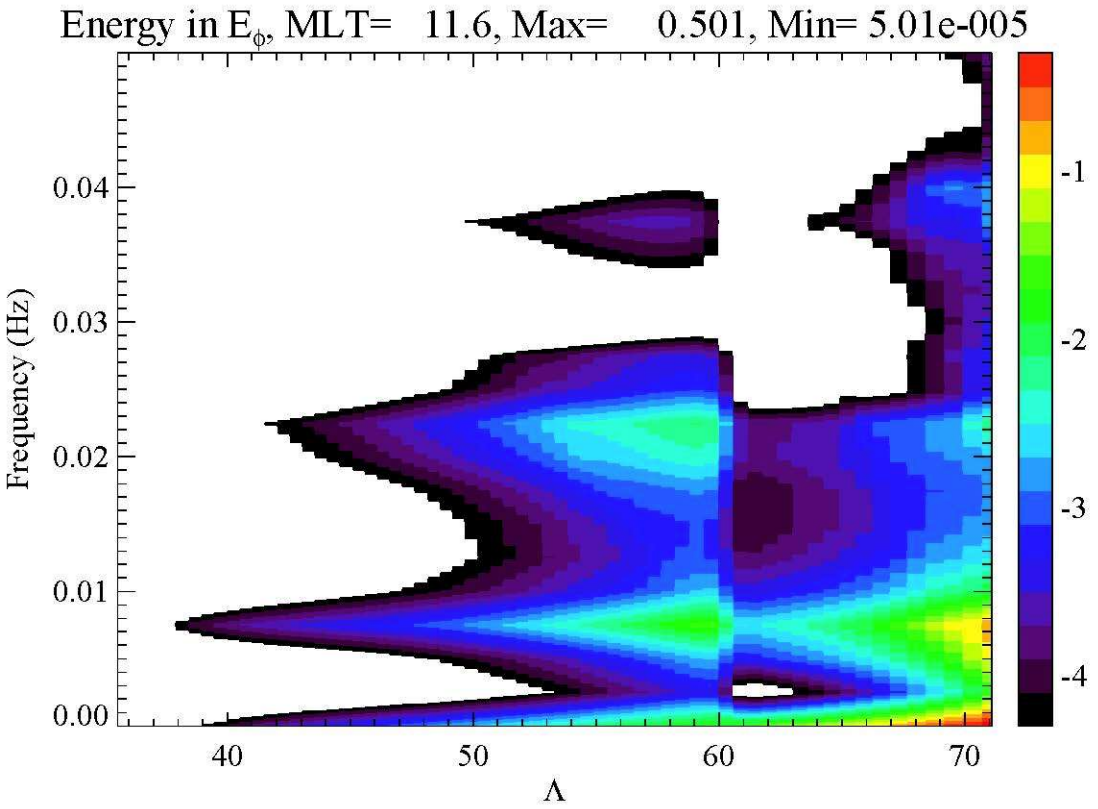

Figure 6. Energy density in the poloidal component of the electric field, showing the cavity mode nature of these oscillations. Note that the cavity mode is not strictly confined to the plasmasphere and in fact leaks out to the outer magnetosphere.

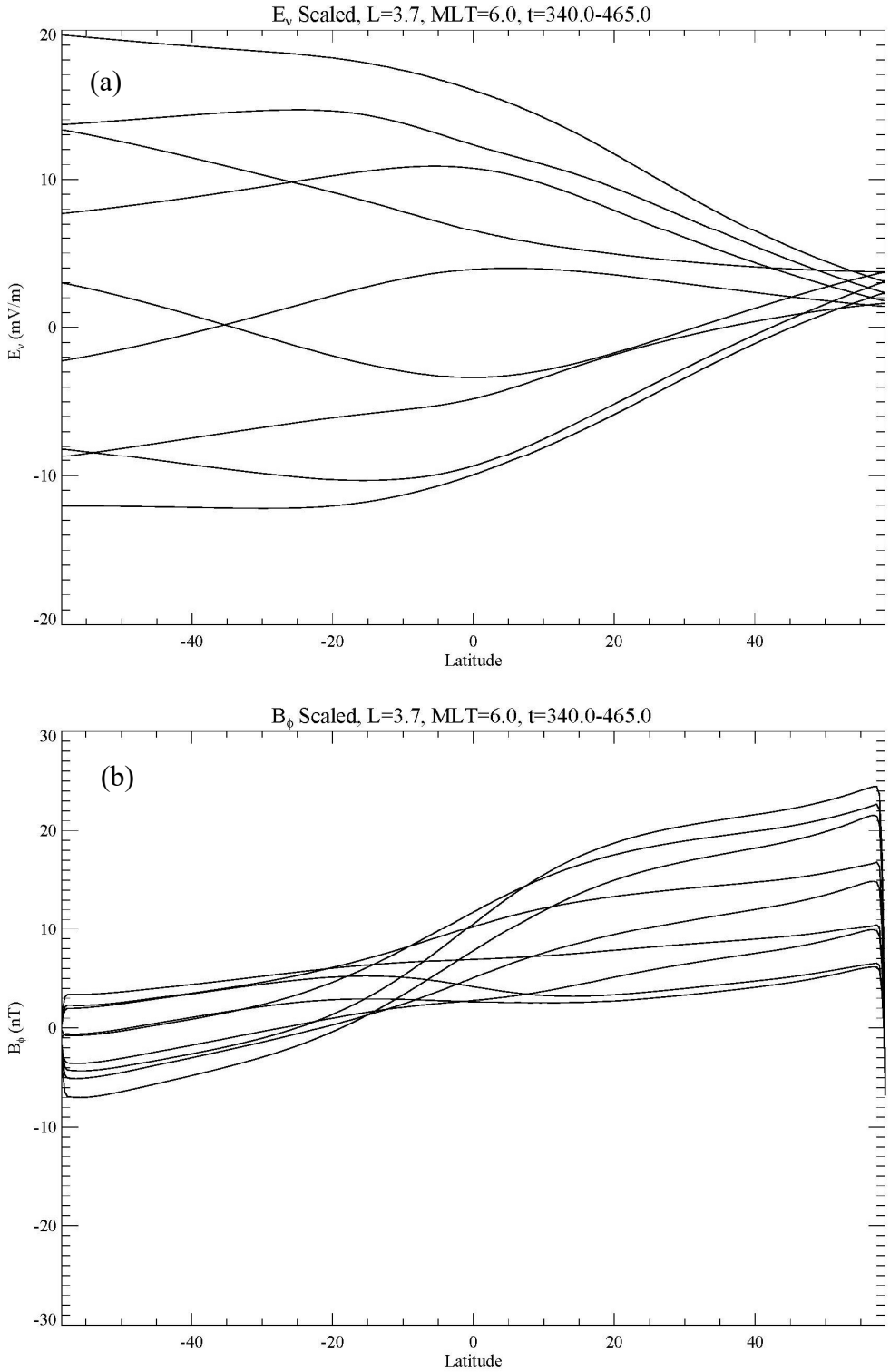

Figure 7. Wave forms of the (a) electric and (b) magnetic fields of the toroidal oscillation as a function of latitude along the magnetic field lines. Note that the fields have been scaled to their ionospheric values.

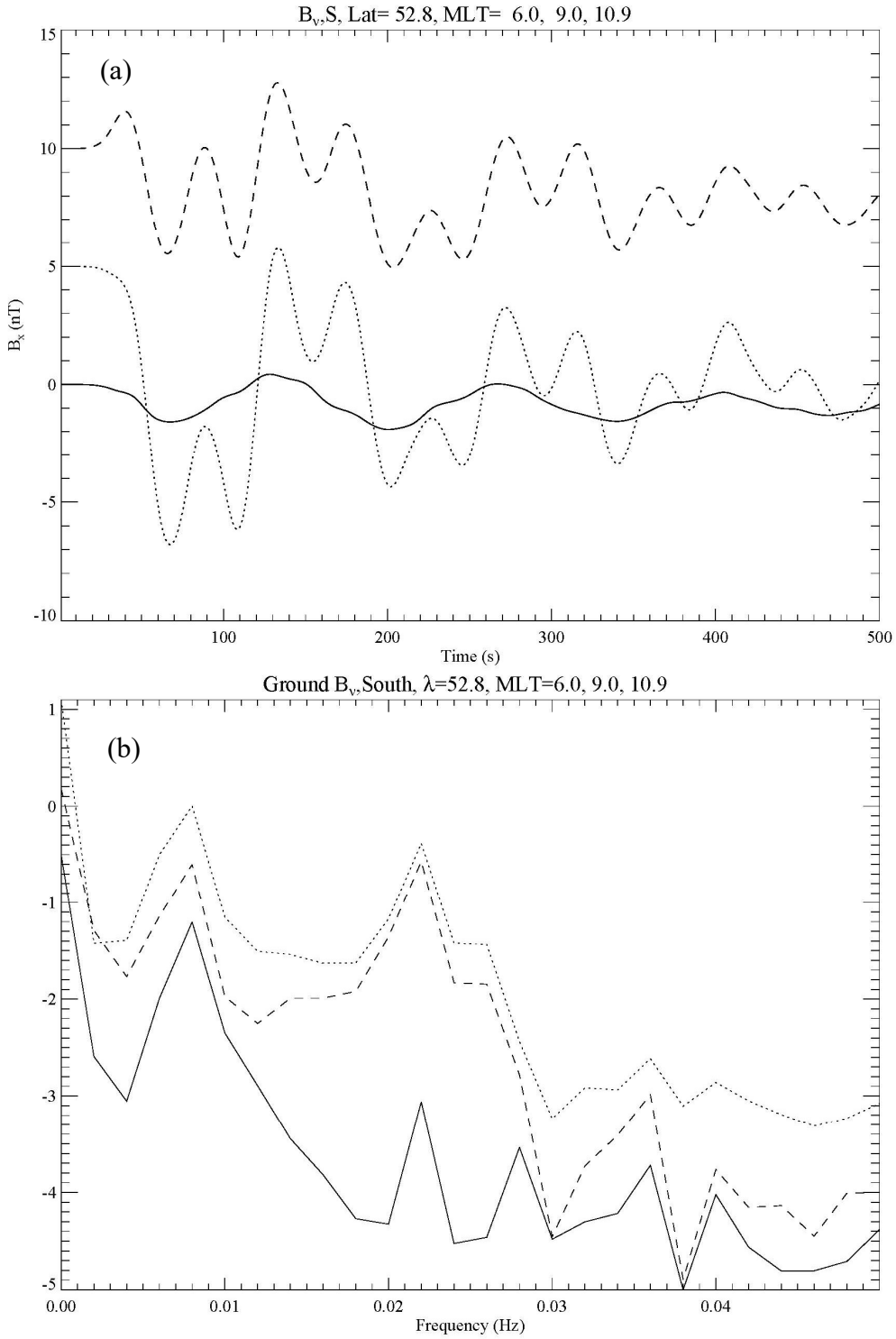

Figure 8. (a) Ground magnetic fields at 52.8° latitude in the southern (dark) ionosphere. The solid line is at 6 MLT, the dotted line at 9 MLT and the dashed line at 11; (b) Fourier transforms of these fields.

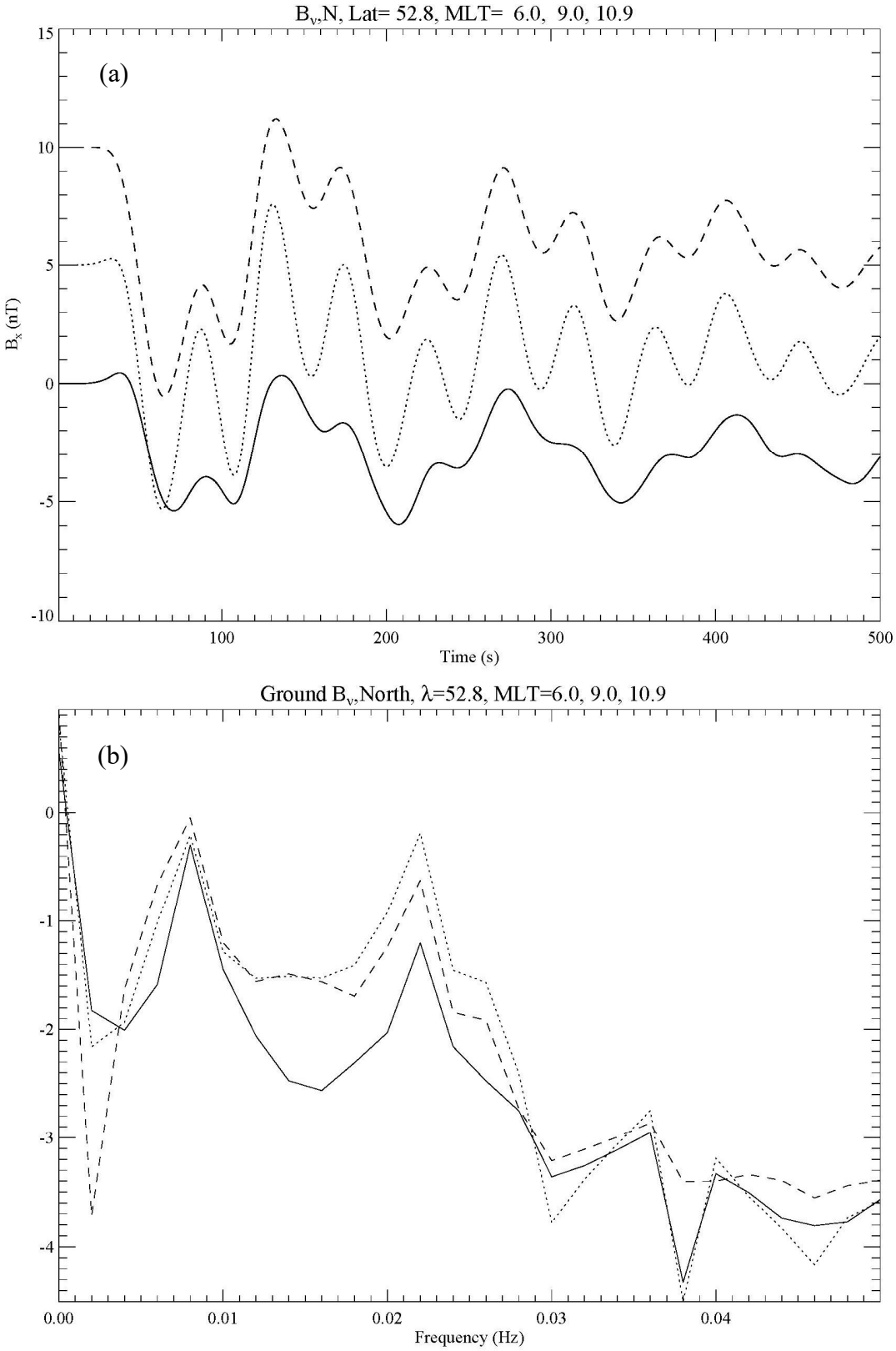

Figure 9. Same as Figure 8, but for the fields in the northern (sunlit) hemisphere.

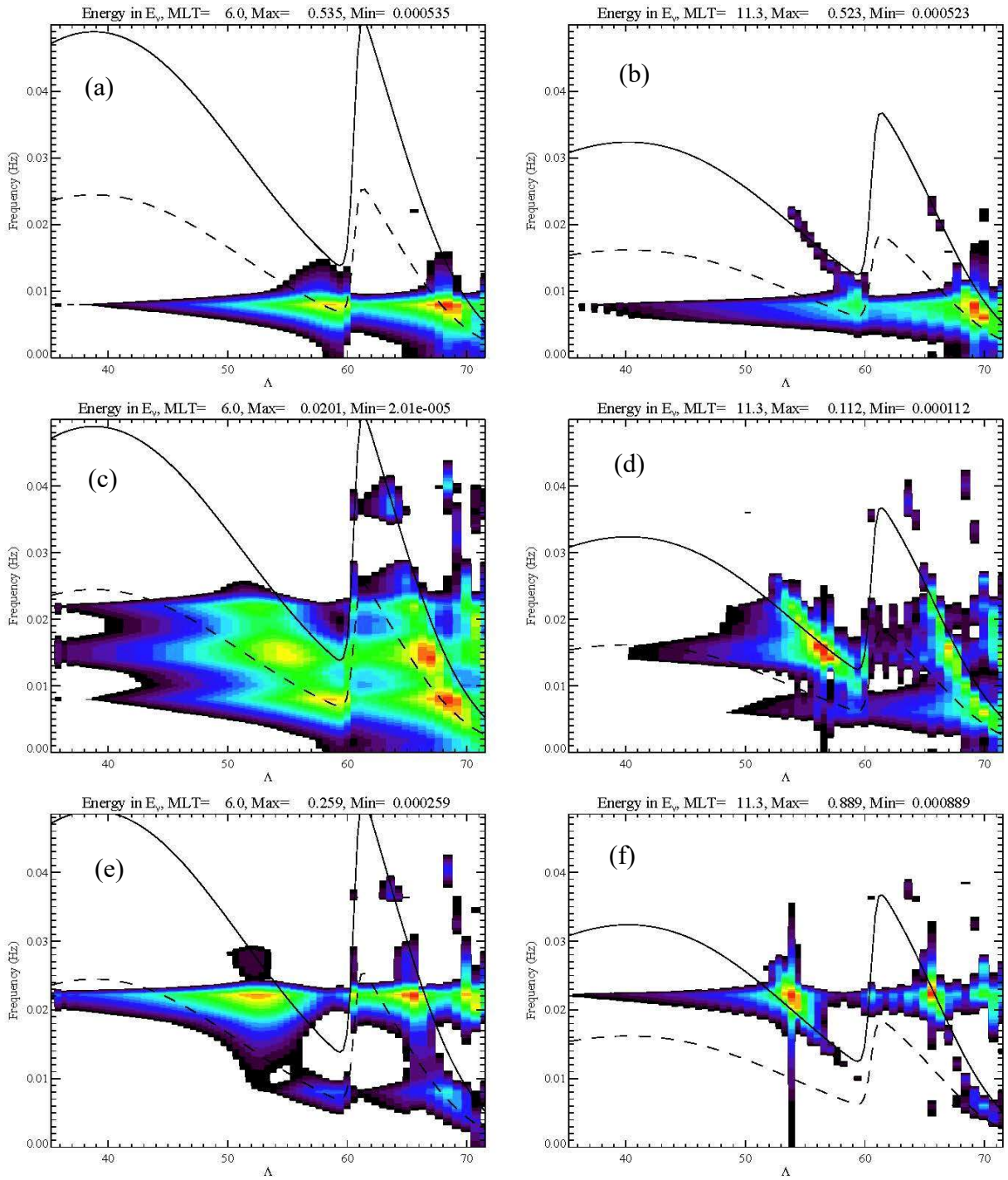

Figure 10. Energy density in the toroidal electric field at 6 MLT (panels a,c, and e) and 11 MLT (panels b, d, and f). Panels (a) and (b) are for a driving frequency of 8 mHz; panels (c) and (d) for 15 mHz and panels (e) and (f) for 22 mHz.

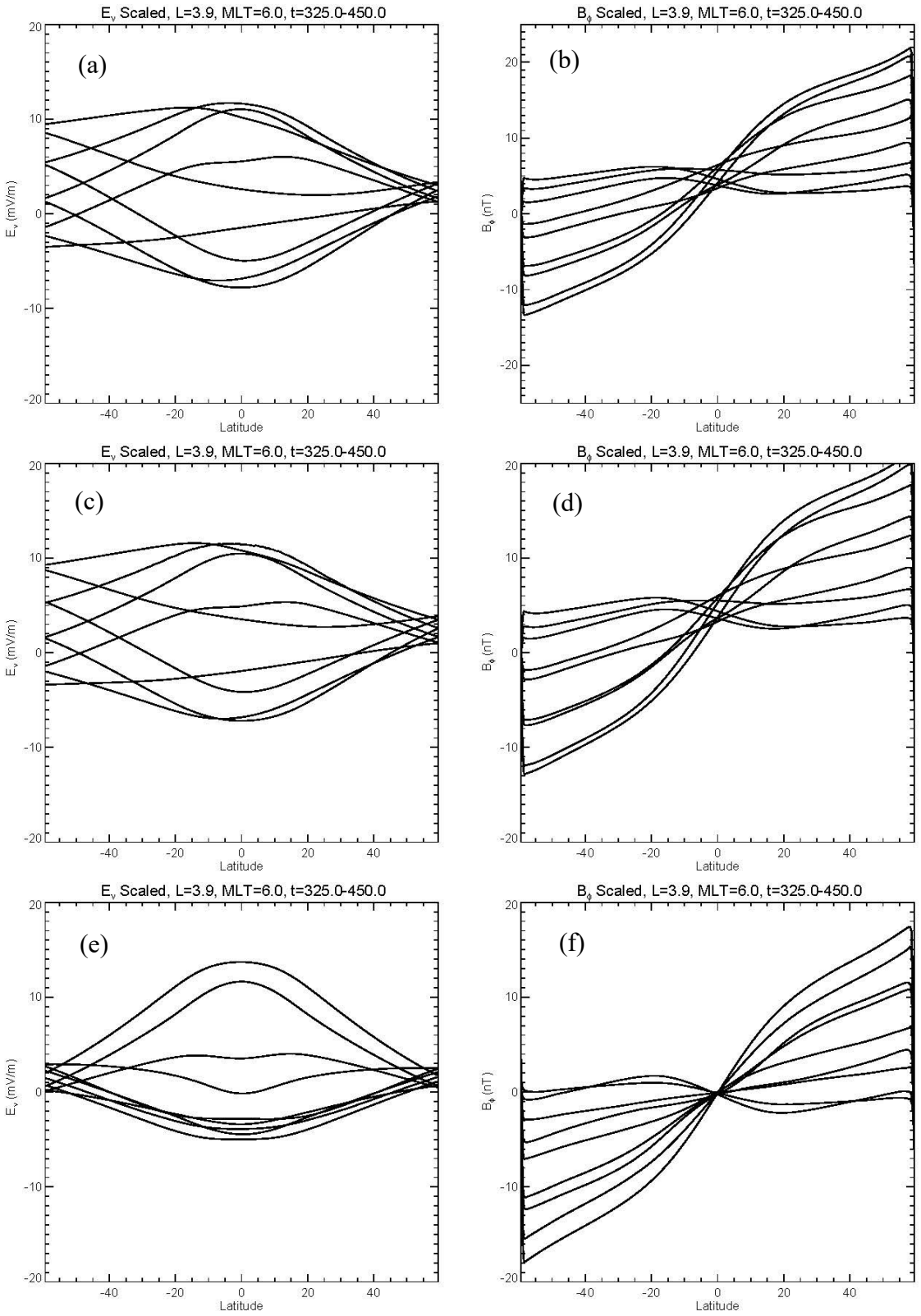

Figure 11. Effect of varying the conductance ratio. Panels (a) and (b) are for a ratio of 11.1, (c) and (d) for 5.4 and (e) and (f) for 2.1. Left column gives the electric field and right column the magnetic field.

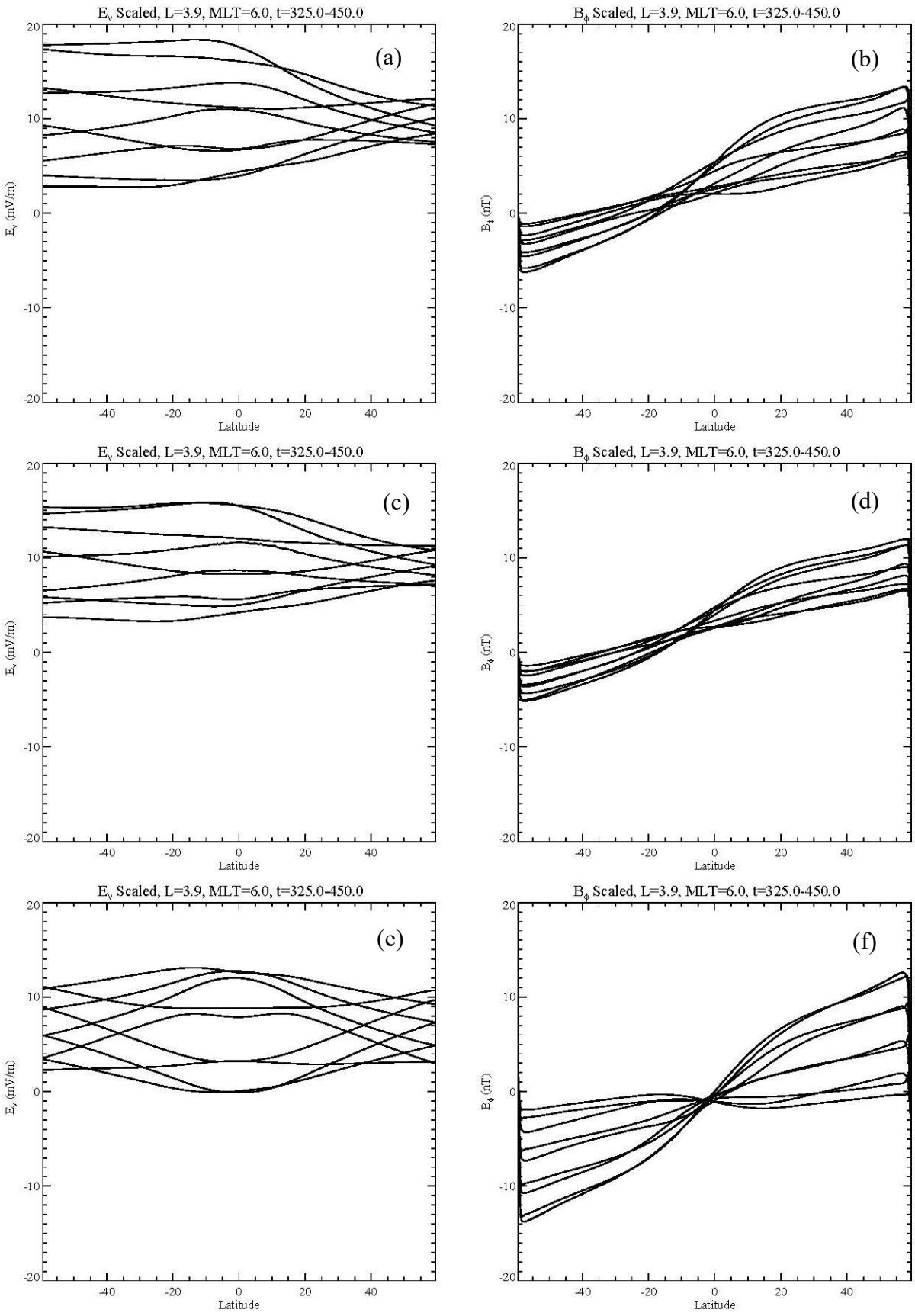

Figure 12. Similar to Figure 11 but for lower conductance values.

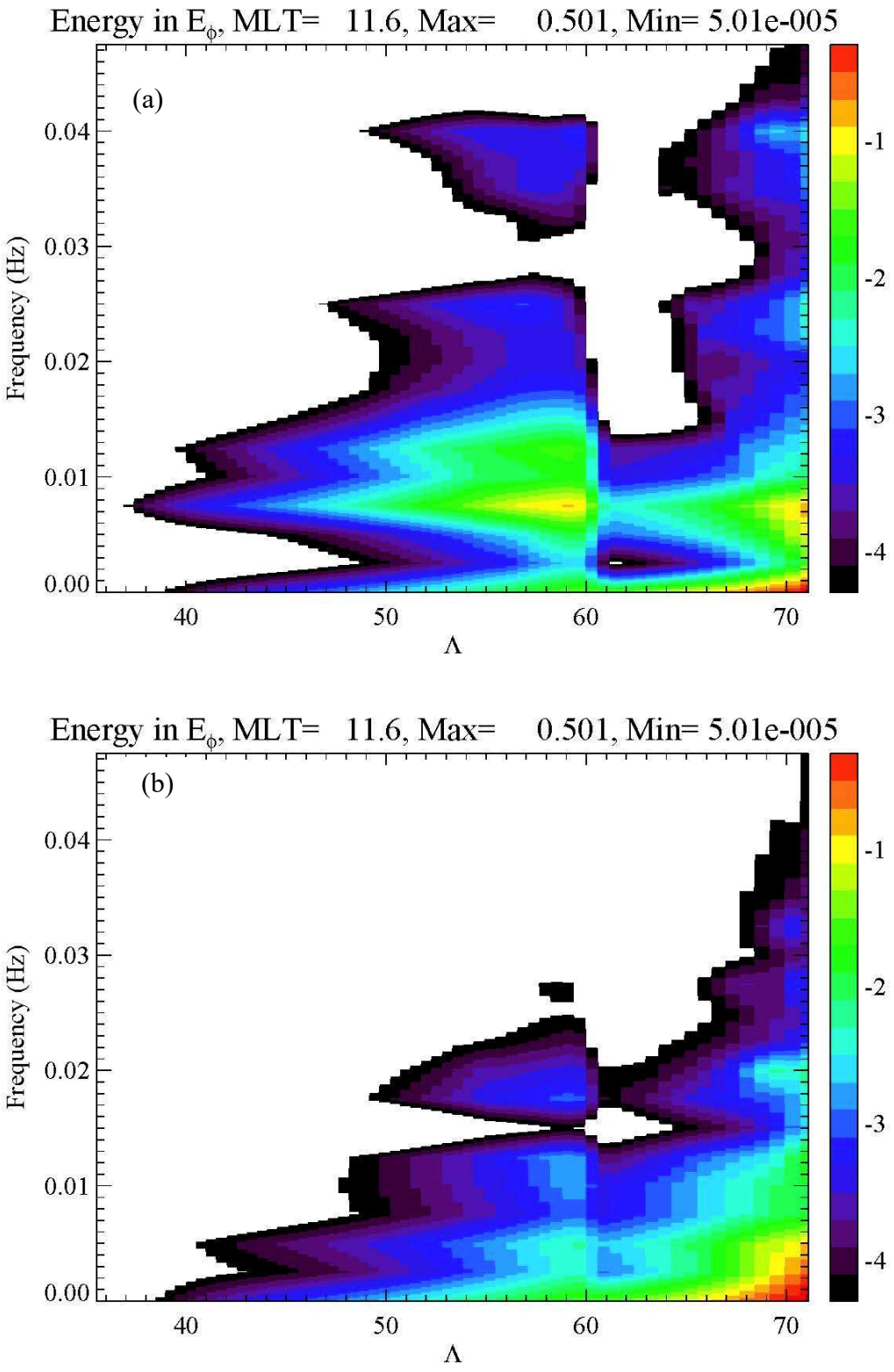

Figure 13. Poloidal energy density in the electric field integrated along the field line for runs in which (a) the plasmaspheric density is increased by a factor of 4, and (b) the outer magnetospheric density is increased by a factor of 4. Note that both modifications affect the energy spectrum; however the frequency decrease is more pronounced in the second case.